

Systematic Raman study of optical phonons in $R\text{Ba}_2\text{Cu}_3\text{O}_{6+\delta}$ ($R = \text{Y, Dy, Gd, Sm, Nd}$): Antiferromagnetic coupling strength versus lattice parameters

Silvia Müllner¹, Wayne Crump², Dirk Wulferding¹, Benjamin P. P. Mallett^{3,4},

Peter Lemmens¹, Amit Keren⁵, and Jeffery L. Tallon^{2,4}

¹*Institute for Condensed Matter Physics, Technical University of Braunschweig, D-38106 Braunschweig, Germany*

²*Robinson Research Institute, Victoria University of Wellington, P.O. Box 33436, Lower Hutt 5046, New Zealand*

³*Physics and Chemical Sciences, Dodd Walls Centre for Photonic and Quantum Technologies, The Photon Factory, University of Auckland, 38 Princes St, Auckland, New Zealand*

⁴*MacDiarmid Institute for Advanced Materials and Nanotechnology, School of Chemical and Physical Sciences, Victoria University of Wellington, PO Box 600, Wellington, New Zealand*

⁵*Department of Physics, Technion-Israel Institute of Technology, Haifa 32000, Israel*

(Dated: April 24, 2019)

We present a systematic study of the interplay between lattice parameters and the energy of the optical phonons as well as the antiferromagnetic coupling strength, J , in the high- T_c superconducting cuprate $R\text{Ba}_2\text{Cu}_3\text{O}_{6+\delta}$ (R -123, $R = \text{Y, Dy, Gd, Sm, Nd}$) with hole doping p ($0.00 < p \lesssim 0.04$). The energy of the B_{1g} mode at $\nu_{B_{1g}} \approx 335 \text{ cm}^{-1}$ has been found to relate systematically to the inverse of the lattice parameter a . Our results confirm the temperature dependent phonon splitting for Nd-123 at low doping, which has been reported for optimally doped Nd-123. Surprisingly, J is independent of a for the first four R families, and a general consistency between T_c^{max} and J , as suggested in a previous investigation, could not be confirmed.

I. INTRODUCTION

$R\text{Ba}_2\text{Cu}_3\text{O}_{6+\delta}$ (R -123) hosts a variety of electronic and magnetic properties. The mechanisms leading to the complexity of its phase diagram, e.g., antiferromagnetic (AFM), pseudogap, metallic, superconducting states are still unresolved [1, 2]. Its physical properties depend on the temperature, and doping, which is controlled by the oxygen content δ [3, 4]. At optimal hole doping ($p \approx 0.16$), it reaches a superconducting transition temperature of $T_c^{\text{max}} \approx 100 \text{ K}$ [5, 6]. At low doping ($p \lesssim 0.05$) it is an AFM Mott insulator [7, 8] with an AFM coupling strength on the order of $J \approx 100 \text{ meV}$ [9, 10]. The Heisenberg model describes the long-range AFM ordering via nearest-neighbor interaction of the spin carriers but does not explain the doping dependence. The generally accepted Hubbard model deals with the doped case although it fails to explain the material dependent systematics, for example, the properties of the refractive sum [11]. The Heisenberg and Hubbard models in their simplest form are related at strong coupling via $J \propto t^2/U$, where t is the hopping parameter and U the on-site interaction.

Our study focuses on the electronic and magnetic properties of R -123 by analyzing the phonon modes and two-magnon scattering from Raman scattering experiments. The required energy for a spin-flip process depends on J and relates to the Raman shift of the two-magnon peak, ν_{2m} [12–15]. Since U is not expected to vary between materials, measurements of J actually reflect on t , a parameter that is relevant at all doping.

The lattice parameters are controlled by the radius of the rare-earth (R) ion, r_R . Our R -123 samples ($R = \text{Y, Dy, Gd, Sm, Nd}$) order antiferromagnetically. The magnetic moment resides on the Cu ion, which lie within the crystallographic ab plane. These samples have a hole-

doping content of p ($0.00 < p \lesssim 0.04$) (see Table I) in which the lattice parameters a and b are equal [16, 17]. Reference values of r_R and the lattice parameter a and c were obtained from a neutron diffraction study by Guillaume *et al.* [18] and are found in Table II.

II. EXPERIMENTAL

Long-range magnetic order decreases with increasing temperature; hence the two-magnon data was collected at $T = 15 \text{ K}$. A helium flow cryostat (KONTI-cryostat-Mikro) cooled the samples in a vacuum environment. The micro-Raman setup (Jobin-Yvon, LabRAM HR) operates with a liquid nitrogen cooled CCD camera (Horiba, Spectrum One) and a Nd:YAG solid-state laser which emits an excitation wavelength of $\lambda_{\text{exc}} = 532.1 \text{ nm}$. The confocal setup with 50x magnification produced a laserspot on the sample with a diameter of $d_{\text{spot}} \approx 10 \mu\text{m}$ and a laser power of $P_{\text{laser}} \approx 150 \mu\text{W}$. We use the Porto notation to describe the light polarization and orientation of the sample. The low temperature measurements were taken in $-z(x'y')z$ backscattering geometry because two-magnon scattering is strongest in B_{1g} symmetry [19].

Each sample is an agglomerate of single crystals of sizes up to $l_{\text{crystal}} \approx 100 \mu\text{m}$. The doping of the crystals has been adjusted by annealing in argon, typically at $T \approx 650 \text{ }^\circ\text{C}$, followed by quenching into liquid nitrogen. In each case, the doping state was determined using measurements of thermoelectric power [20] (i.e., Seebeck coefficient) at room temperature, $S_{290} = 372 \exp(-32.4p)$ [21], and confirmed to be close to zero hole doping. Since the two-magnon Raman shift can be analyzed in terms of the Heisenberg model only in the undoped case, the lightly doped samples allow us to either verify that our results are doping independent

or extrapolate them to zero doping if needed.

TABLE I. Our investigated R -123 samples.

R -123	p (holes per Cu atom)
Y-123	0.027, 0.017, 0.000
Dy-123	0.026, 0.023, 0.020, 0.001, 0.000
Gd-123	0.024, 0.017, 0.003, 0.001, 0.000
Sm-123	0.024, 0.020, 0.006, 0.000
Nd-123	0.036, 0.025, 0.000

III. RESULTS AND DISCUSSION

The orientation of the crystal has been determined by polarization dependent measurements at room temperature, in which each sample was rotated in steps of approximately 15° and measured sequentially; see Fig. 1(a). The highest scattering intensity of the mode at $\nu_{B_{1g}} \approx 335 \text{ cm}^{-1}$ determines the B_{1g} geometry, whilst the low intensity of this mode at 0° (and symmetry related angles) indicates good crystallinity within the measurement area. Figure 1(b) shows the phonon spectra of different R -123. Each hosts a mode at $\nu_{B_{1g}} \approx 335 \text{ cm}^{-1}$ involving antiphase vibrations of the oxygen ions in the CuO_2 layers. A broad mode with weak intensity emerges at $\nu \approx 198 \text{ cm}^{-1}$ in Sm-123 and also in Gd-123, Dy-123, and Y-123. This mode has been observed in previous studies on AFM Y-123 [22]. Our polarization dependent measurement, see Fig. 1(a), shows that this mode has A_{1g} character.

Some additional modes appear around $\nu \approx 450 \text{ cm}^{-1}$, 500 cm^{-1} , and 600 cm^{-1} and are associated with, respectively, in-phase O vibration on the CuO_2 sites, O vibration on the apical site, and O vibration on the Cu-O chain sites [23, 24]. The A_{1g} mode at $\nu_{A_{1g}} \approx 145 \text{ cm}^{-1}$ involves vibrations of the in-plane Cu ions [25]. In Nd-123, this mode is only observed at $p \approx 0.00$ [see Fig. 1(c)]. The absence of the A_{1g} mode with even slightly higher p correlates with the phonon splitting of the B_{1g} mode in Nd-123. This phonon splitting has been observed in optimally doped Nd-123 [26–28]. It is ascribed to the coupling and mixing of the B_{1g} mode to a crystal-field excitation that involves a $\text{Nd}^{3+} 4f$ electron. Our data confirms this splitting between ($0.02 \lesssim p \lesssim 0.04$) in which the modes have a Raman shift of $\nu_{B_{1g}} \approx 332 \text{ cm}^{-1}$ and $\nu_{\text{ph}} \approx 274 \text{ cm}^{-1}$. No such splitting is observed at $p \approx 0.00$ and all temperatures. With increasing p , the structure of Nd-123 might become more susceptible to changes and phonon-crystal-field splitting. An anomalous shift of the phonon crystal-field excitation at room temperature is observed throughout the investigated doping region, i.e., the phonon has a Raman shift of $\nu_{B_{1g}} \approx 317 \text{ cm}^{-1}$ instead of $\nu_{B_{1g}} \approx 332 \text{ cm}^{-1}$ as illustrated in Fig. 1(c).

Figure 1(d) depicts the two-magnon spectra with the peak position at ν_{2m} . For spin $S = 1/2$ systems, as present in the examined samples, J relates to ν_{2m} with $J = \nu_{2m}/3.22$ [12, 13], $J = \nu_{2m}/2.8$ [14],

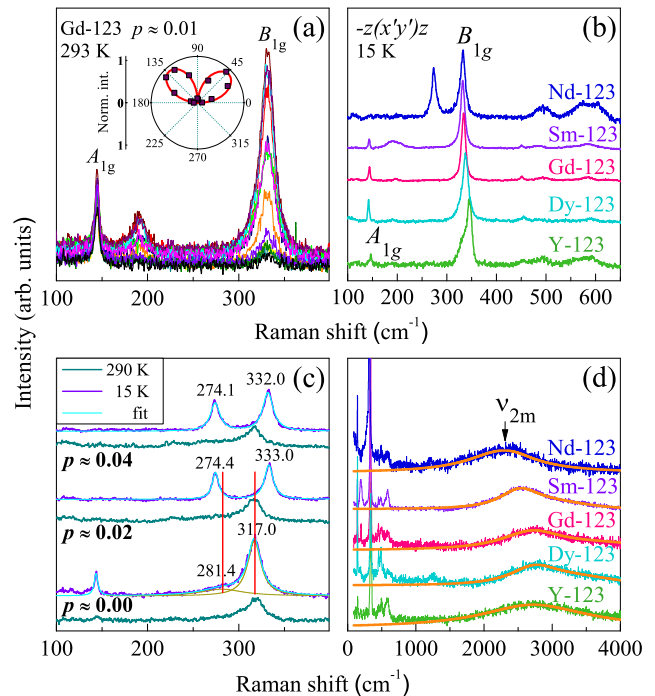


FIG. 1. (a) Raman spectra of Gd-123 in different light polarizations. The integrated intensity of the B_{1g} mode is fitted with a sine function (inset). (b) Phonon spectra of different R -123. (c) Nd-123 at different p and T . (d) Two-magnon excitation at ν_{2m} from different R -123, fitted with a Lorentzian and an additional Gaussian function.

or $J = \nu_{2m}/2.84$ [15] depending on the theoretical approach; we chose the first one to be consistent with Ref. [29]. The peaks are predominantly fitted with a Lorentzian function and an additional Gaussian function towards the higher Raman shift region of ν_{2m} . We ascribe this to contributions from magnons and electrons, respectively [30].

Figure 2(a) shows the Raman shift of the B_{1g} mode, $\nu_{B_{1g}}$. The data points are assigned to a certain symbol and color, corresponding to the R ion. The Raman shift of the B_{1g} mode remains unaffected within our investigated doping region, illustrated with the shaded areas. The inset of Fig. 2(a) depicts spectra of the B_{1g} mode from Nd-123, Sm-123, Gd-123, Dy-123, and Y-123 (left to right). The Raman shift of the two modes, $\nu_{B_{1g}}$ and $\nu_{A_{1g}}$, are listed in Table II and are plotted versus the lattice parameter a in Fig. 2(b). The Raman shift of the B_{1g} mode monotonically decreases with increasing lattice parameter a in agreement with previous studies [31]. We find that it relates to a according to

$$\nu_{B_{1g}} = \left[\frac{0.048}{a - 3.853} + 330.64 \right] \text{ cm}^{-1}.$$

The A_{1g} mode has a similar trend with a larger margin of error due to the weak scattering intensity of this mode.

The analysis seen in Fig. 2(b) demonstrates that the

Raman shift of the B_{1g} mode undergoes a greater change with a than the A_{1g} mode. A possible explanation for this might be the proximity of the modes to the R ion, because the radius of the R ion is varied to tune the lattice parameters. The B_{1g} mode is about half the distance to the R ion than the A_{1g} mode. Also noteworthy is the lower limit of the B_{1g} mode at $\nu_{B_{1g}, \min} \approx 331 \text{ cm}^{-1}$ towards larger a .

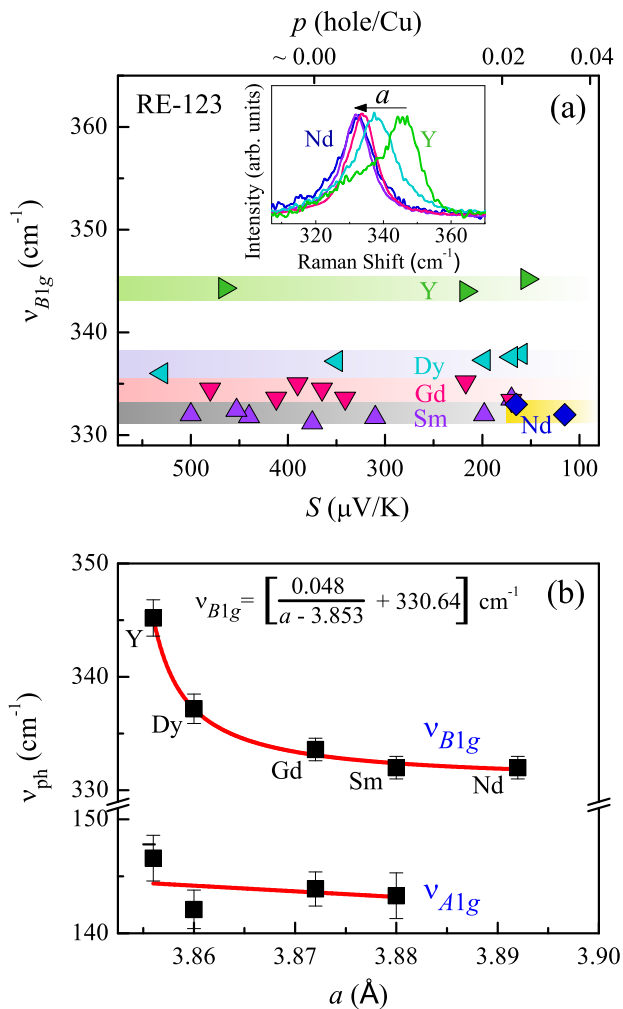


FIG. 2. (Inset) B_{1g} mode of different R -123. (a) Raman shift of the B_{1g} mode plotted versus the doping p , which is associated with S . (b) Average Raman shift of the A_{1g} and B_{1g} modes for the different R -123 compared with the lattice parameter a . The B_{1g} mode is fitted with the indicated function and the A_{1g} mode has a linear fit.

As seen in Fig. 1(d), the Raman shift of ν_{2m} is only marginally affected within the investigated doping range. Generally, the two-magnon peak hardens with decreasing doping and is consistent with previous studies on other high- T_c SC cuprates [34–36]). This trend is illustrated with the shaded areas in Fig. 3(a) for Dy-123, Sm-213 and Nd-123. The yellow shaded area indicates the region for $p \approx 0.00$ ($S \gtrsim 340 \mu\text{V/K}$). From this region, the

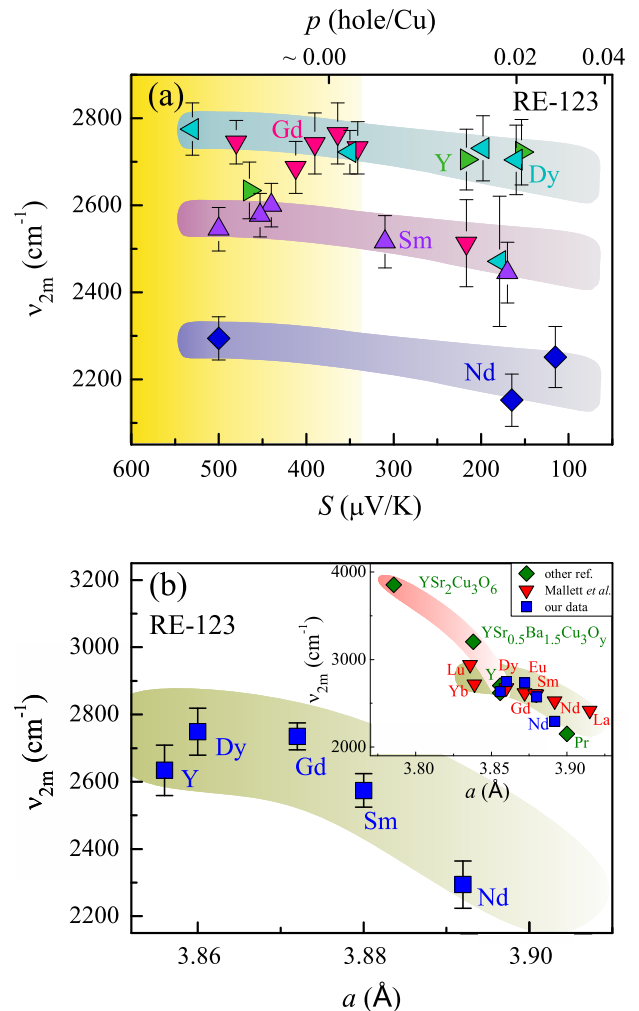


FIG. 3. (a) Two-magnon peak, ν_{2m} , versus doping, p , and thermoelectric power, S . The yellow region indicates $p \approx 0.00$ and the shaded areas illustrate the trend towards lower ν_{2m} with increasing p , in e.g., Dy-123, Sm-123, and Nd-123. (b) Average values of ν_{2m} of each R -123 taken from the yellow shaded area in (a) and plotted versus a . (Inset) Our data (blue squares) and other data (red triangles and green diamonds) to cover the widest possible data range [29, 33].

average value of ν_{2m} for each R -123 is plotted versus a in Fig. 3(b) and is listed in Table II as well. The olive green shaded area shows the systematic relation between ν_{2m} and a . The surprising result is that from Y-123 to Sm-123 there is no change in ν_{2m} within experimental errors and only for Nd-123 a downward trend is observed. This stands in contrast to the systematic behavior of the B_{1g} mode. J is independent of a for four out of five samples we reexamined.

Reference values of ν_{2m} for $\text{YSr}_2\text{Cu}_3\text{O}_6$ [33], $\text{YSr}_{0.5}\text{Ba}_{1.5}\text{Cu}_3\text{O}_6$ [26, 29], and other lanthanide (Ln) Ln-123 are considered in the inset of Fig. 3(b) shown with green diamonds and red triangles [29] in order to cover the widest possible range for J versus a . These

TABLE II. Literature values of r_R , a , b , c , T_c^{\max} and buckling angle on CuO_2 plane of R -123 for $p < 0.05$ [5, 6, 18, 29]. Our data is indicated with an asterisk. Our v_{2m} and some reference values of v_{2m} [29, 32] are converted to J [12].

R -123	r_R (Å)	a, b (Å)	c (Å)	T_c^{\max} (K)	buckling angle a/b-axis ($^\circ$)	v_{A1g}^* (cm^{-1})	v_{B1g}^* (cm^{-1})	v_{2m}^* (cm^{-1})	reference v_{2m} (cm^{-1})	J (meV)
Y-123	1.019	3.856	11.793	93.5	6.2	146.6	345.2	2634	2615	101.5*
Dy-123	1.027	3.860	11.796	92.2	6.04	142.1	337.2	2749	2678	105.8*
Gd-123	1.053	3.872	11.807	93.6	6.06	143.9	333.6	2735	2620	105.3*
Eu-123	1.066	3.879	11.811	94.0	5.43	n.a.	n.a.	n.a.	2610	100.5
Sm-123	1.079	3.880	11.815	94.7	5.63	143.3	332.0	2574	2605	99.1*
Nd-123	1.109	3.893	11.830	96.1	6.90	n.a.	332.1	2294	2525	88.3*
Pr-123	1.126	3.900	11.832	n.a.	6.06	n.a.	n.a.	n.a.	2190	84.3

compounds have the same structure as R -123. However, $\text{YSr}_2\text{Cu}_3\text{O}_6$ is synthesized under high oxygen pressure [33, 37] and, along with $\text{YSr}_{0.5}\text{Ba}_{1.5}\text{Cu}_3\text{O}_6$, is more compressed because Sr is substantially smaller than Ba while the compounds are otherwise isostructural with Y-123. Nevertheless, the different out-of-plane structure possibly renders these last two compounds in a class on their own. The green and pink shaded areas in the inset of Fig. 3(b) emphasize these two classes yet together they show a systematic decrease of v_{2m} with increasing a for R -123, but perhaps with different rates. As Y-123 is not part of the lanthanide series plus the fact that its orbital structure differs slightly from the Ln-123, it is not clear to which class it belongs (green or pink). Hence it is represented in both areas. The uniqueness of Y might be the reason for the different a dependence of v_{2m} in the pink area compared with the remaining Ln-123. The apical oxygen bond length could be a crucial factor that influences J [38] and might account for the low value of J in the Y-123 compared with the other Y based compounds. Beyond that we need to recognize that any small variations may be attributable to compositional or doping variations, particularly noting that Raman and thermopower effectively probe different depths in samples where we have attempted, with difficulty, to remove the last dopant oxygen.

Studies on whether J relates to T_c^{\max} have led to conflicting findings. Wulferding *et al.* observed, using Raman, a linear increase of T_c^{\max} with increasing J in $(\text{Ca}_x\text{La}_{1-x})(\text{Ba}_{1.75-x}\text{La}_{0.25+x})\text{Cu}_3\text{O}_y$ (CLBLCO), an isostructural compound to R -123, and proposed a correlation between these parameters [34]. Their measurements are in agreement with J determination by muon spin rotation [39], resonance inelastic x-ray scattering [40], and with t measurement by angle resolved photoemission spectroscopy [41]. On the other hand, Mallett *et al.* observed a decreasing T_c^{\max} with J but also found the opposite behavior when applying external pressure on R -123 [29, 42]. Both, the data of Wulferding *et al.* and Mallett *et al.* regarding T_c^{\max} versus J are compared to our data in Fig. 4. The data of Mallett *et al.* is in good agreement with our data (apart from the Nd-123 sample). The contradicting result of Wulferding *et al.* to the other two results suggests that no general conclusion between

T_c^{\max} and J can be drawn based on Fig. 4. Reasons for this contradiction have been proposed [42].

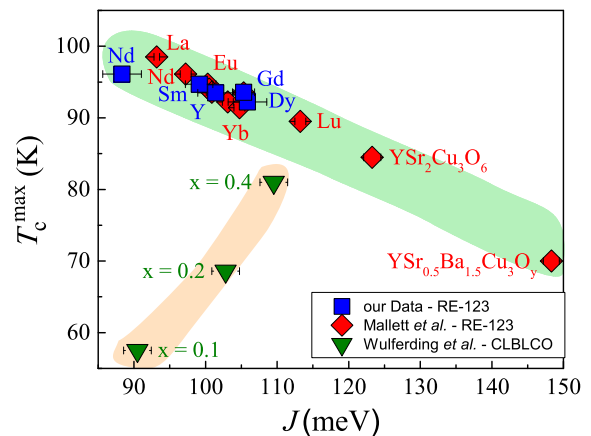


FIG. 4. Maximum transition temperature T_c^{\max} as a function of the AFM coupling strength, J [12, 14, 15], of R -123 in the green shaded area. The red diamonds and blue squares are data from Mallett *et al.* [29] and us, respectively. The $\text{YSr}_2\text{Cu}_3\text{O}_6$ and $\text{YSr}_{0.5}\text{Ba}_{1.5}\text{Cu}_3\text{O}_6$ were synthesized under high pressure [33, 37]. The green triangle shows data of an isostructural compound to R , $(\text{Ca}_x\text{La}_{1-x})(\text{Ba}_{1.75-x}\text{La}_{0.25+x})\text{Cu}_3\text{O}_y$ (CLBLCO) from Wulferding *et al.* [34].

IV. SUMMARY

A systematic relation between the energy of the optical phonons and the lattice parameter a could be determined. In previous studies a T -dependent phonon splitting of the B_{1g} mode was observed in optimally-doped Nd-123 [27, 28]. Our results confirm this splitting for low hole doping, but not for undoped Nd-123. For the samples we reexamined, the AFM coupling strength, J , did not decrease monotonically with increasing lattice parameter a . When considering other studies, including samples prepared under high pressure, a general trend of decreasing J with increasing a becomes apparent, al-

though with a plateau around $a = 3.85 \text{ \AA}$. A universal relation between T_c^{max} and J as suggested previously [34] could not be established.

V. ACKNOWLEDGEMENTS

This work has been made possible by the support of the Deutsche Forschungsgemeinschaft DFG Grant No.

LE967/16-1 and QUANOMET initiative within Project LENA-NL4-1, and by the German-Israeli Foundation for Scientific Research and Development (GIF). BPPM acknowledges support from the Rutherford Foundation of New Zealand. We thank Kim Paul Schmidt, Dr. Roser Valentí and Bo Liu for constructive discussions.

-
- [1] B. Keimer, S. A. Kivelson, M. R. Norman, S. Uchida, and J. Zaanen *Nature*, vol. 518, pp. 179–186, (2015).
- [2] J. G. Bednorz and K. A. Müller *Z. Phys. B*, vol. 64, (1986). pp. 189–193.
- [3] R. Cava *Science*, vol. 247, pp. 656–662, (1990). Provided by the SAO/NASA Astrophysics Data System.
- [4] J. D. Jorgensen, P. Lightfoot, and S. Pei *Superconductor Science and Technology*, vol. 4, no. 1S, pp. 11–18, (1991).
- [5] *Physica C: Superconductivity*, vol. 204, no. 3, pp. 237–246.
- [6] B. W. Veal, A. P. Paulikas, J. W. Downey, H. Claus, K. Vandervoort, G. Tomlins, H. Shi, M. Jensen, and L. Morss *Physica C*, vol. 97, pp. 162–164, (1989).
- [7] R. Wesche, *Physical Properties of High Temperature Superconductors*. The Atrium, Southern Gate, Chichester, West Sussex, PO19 8SQ, UK: John Wiley & Sons, Ltd, (2015). p. 482.
- [8] P. A. Lee, N. Nagaosa, and X.-G. Wen *Rev. Mod. Phys.*, vol. 78, pp. 17–85, (2006).
- [9] R. Birgenau and G. Shirane, *Physical Properties of High Temperature Superconductors I*. P O Box 128, Farrer Road, Singapore 9128: World Scientific Publishing Co. Pte. Ltd, (1989). pp. 151–153.
- [10] S. Sugai, M. Sato, T. Kobayashi, J. Akimitsu, T. Ito, H. Takagi, S. Uchida, S. Hosoya, T. Kajitani, and T. Fukuda *Phys. Rev. B*, vol. 42, pp. 1045–1047, (1990).
- [11] R. Shannon *Journal of Applied Physics*, vol. 73, pp. 348–366, (1993).
- [12] J. B. Parkinson *Journal of Physics C: Solid State Physics*, vol. 2, no. 11, pp. 2003–2011, (1969).
- [13] A. V. Chubukov and D. M. Frenkel *Phys. Rev. B*, vol. 52, pp. 9760–9783, (1995).
- [14] A. V. Chubukov and D. M. Frenkel *Phys. Rev. Lett.*, vol. 74, pp. 3057–3060, (1995).
- [15] S. A. Weidinger and W. Zwirger *Eur. Phys. J. B*, vol. 88, (2015).
- [16] M. Glazer and A. N. G. G. Burns, *Space Groups for Solid State Scientists*. 1250 Sixth Avenue, San Diego, CA 92101: Academic Press, Inc., (1990). p. 263.
- [17] Z.-X. Chai and Y. Zhu, *Microstructures and Structural Defects in High-temperature Superconductors*. Brookhaven National Laboratory Upton, New York, USA: World Scientific Publishing Co. Pte. Ltd., (1998). p. 46.
- [18] M. Guillaume, P. Allenspach, W. Henggeler, J. Mesot, B. Roessli, U. Staub, P. Fischer, A. Furrer, and V. Trounov *Journal of Physics: Condensed Matter*, vol. 6, no. 39, p. 7963, (1994).
- [19] N. Chelwani and *et al. Phys. Rev. B*, vol. 97, p. 024407, (2018).
- [20] S. D. Obertelli, J. R. Copper, and J. L. Tallon *Phys. Rev. B*, vol. 46, no. 22, pp. 14928–14931, (1992).
- [21] J. L. Tallon, C. Bernhard, H. Shaked, R. L. Hitterman, and J. D. Jorgensen *Phys. Rev. B*, vol. 51, pp. 12911–12914, (1995).
- [22] H. Kuzmany, M. Mehring, and J. Jink, *Electronic Properties of High- T_c Superconductors*. Tiergartenstrasse 17, D-69121 Heidelberg, Germany: Springer-Verlag, (1992). p. 218.
- [23] W. H. Weber and R. Merlin, *Raman Scattering in Material Science*. Tiergartenstrasse 17, D-69121 Heidelberg, Germany: Springer-Verlag, (2000). p. 162–165.
- [24] M. F. Limonov, S. Tajima, and A. Yamanaka *Phys. Rev. B*, vol. 62, pp. 11859–11863, (2000).
- [25] R. Bhattacharya and M. P. Paranthaman, *High Temperature Superconductors*. Reading, Massachusetts: WILEY-VCH Verlag GmbH and Co. KGaA, (2006). p. 100.
- [26] B. P. P. Mallet, *Ion-size effects on cuprate High Temperature Superconductors*. PhD thesis, Victoria University of Wellington, (2013).
- [27] E. T. Heyen, R. Wegerer, and M. Cardona *Phys. Rev. Lett.*, vol. 67, pp. 144–147, (1991).
- [28] E. T. Heyen, R. Wegerer, E. Schönherr, and M. Cardona *Phys. Rev. B*, vol. 44, pp. 10195–10205, (1991).
- [29] B. P. P. Mallett, T. Wolf, E. Gilioli, F. Licci, G. V. M. Williams, A. B. Kaiser, N. W. Ashcroft, N. Suresh, and J. L. Tallon *Phys. Rev. Lett.*, vol. 111, (2013). p. 237001.
- [30] T. P. Devereaux and R. Hackl *Rev. Mod. Phys.*, vol. 79, p. 176, (2007).
- [31] B. Friedl, C. Thomsen, and M. Cardona *Phys. Rev. Lett.*, vol. 65, pp. 915–918, (1990).
- [32] D. Budelmann, J. Holmlund, J. Andreasson, H. Rodríguez, J. Bäckström, L. Börjesson, H. Adrian, U. Merkt, and M. Rübhausen *Phys. Rev. B*, vol. 67, p. 140507, (2003).
- [33] E. Gilioli, A. Gauzzi, T. Besagni, F. Licci, M. Marezio, and P. G. Radaelli *International Journal of Modern Physics B*, vol. 14, pp. 2658–2663, (2000).
- [34] D. Wulferding, M. Shay, G. Drachuck, R. Ofer, G. Bazalitsky, Z. Salman, P. Lemmens, and A. Keren *Phys. Rev. B*, vol. 90, p. 104511, (2014).
- [35] S. Sugai, H. Suzuki, Y. Takayanagi, T. Hosokawa, and N. Hayamizu *Phys. Rev. B*, vol. 68, p. 184504, 2003.
- [36] W. Brenig *Physics Reports*, vol. 251, no. 3, (1995).
- [37] E. Gilioli, P. G. Radaelli, A. Gauzzi, F. Licci, and M. Marezio *Physica C*, vol. 341–348, p. 605, (2000).

- [38] N. A. Bogdanov, S. S. Manni, G. L. and, O. Gunnarsson, and A. Alavi, “New superexchange paths due to breathing-enhanced hopping in corner-sharing cuprates.” (2018).
- [39] R. Ofer, G. Bazalitsky, A. Kanigel, A. Keren, A. Auerbach, J. S. Lord, and A. Amato *Phys. Rev. B*, vol. 74, p. 220508, (2006).
- [40] D. S. Ellis, Y.-B. Huang, P. Olalde-Velasco, M. Dantz, J. Pelliciani, G. Drachuck, R. Ofer, G. Bazalitsky, J. Berger, T. Schmitt, and A. Keren *Phys. Rev. B*, vol. 92, p. 104507, (2015).
- [41] G. Drachuck, E. Razzoli, R. Ofer, G. Bazalitsky, R. S. Dhaka, A. Kanigel, M. Shi, and A. Keren *Phys. Rev. B*, vol. 89, p. 121119, (2014).
- [42] J. L. Tallon *Phys. Rev. B*, vol. 90, p. 214523, (2014).